Hindawi
Journal of Nanomaterials
Volume 2017, Article ID 5970540, 18 pages
https://doi.org/10.1155/2017/5970540

Research Article

Donor Impurity-Related Optical Absorption in GaAs Elliptic-Shaped Quantum Dots

M. A. Londoño,[1] R. L. Restrepo,[2] J. H. Ojeda,[3] Huynh Vinh Phuc,[4] M. E. Mora-Ramos,[5] E. Kasapoglu,[6] A. L. Morales,[7] and C. A. Duque[7]

[1]*Instituto de Matemáticas, Facultad de Ciencias Exactas y Naturales, Universidad de Antioquia UdeA, Calle 70 No. 52-21, Medellín, Colombia*
[2]*Universidad EIA, CP 055428, Envigado, Colombia*
[3]*Grupo de Física de Materiales, Universidad Pedagógica y Tecnológica de Colombia, Tunja, Colombia*
[4]*Division of Theoretical Physics, Dong Thap University, Dong Thap, Vietnam*
[5]*Centro de Investigación en Ciencias-IICBA, Universidad Autónoma del Estado de Morelos, Av. Universidad 1001, 62209 Cuernavaca, MOR, Mexico*
[6]*Faculty of Science, Department of Physics, Cumhuriyet University, 58140 Sivas, Turkey*
[7]*Grupo de Materia Condensada-UdeA, Instituto de Física, Facultad de Ciencias Exactas y Naturales, Universidad de Antioquia UdeA, Calle 70 No. 52-21, Medellín, Colombia*

Correspondence should be addressed to C. A. Duque; cduque_echeverri@yahoo.es

Received 6 December 2016; Accepted 6 March 2017; Published 5 April 2017

Academic Editor: Sergio Bietti

The conduction band and electron-donor impurity states in elliptic-shaped GaAs quantum dots under the effect of an externally applied electric field are calculated within the effective mass and adiabatic approximations using two different numerical approaches: a spectral scheme and the finite element method. The resulting energies and wave functions become the basic information needed to evaluate the interstate optical absorption in the system, which is reported as a function of the geometry, the electric field strength, and the temperature.

1. Introduction

Semiconductor elliptical quantum dots (QDs) have been the subject of investigation for a number of years due to their prospective applications in optoelectronics. Recent works on electronics and optical properties in this kind of nanosystems can be referred to in [1–10]. Among them it is worth highlighting, for instance, the practical realization of elliptical QDs in the InGaN/GaN system which can be used as single photon sources, allowing predefining photon states according to the QD orientation [9]. This points at the prospective applications of this kind of nanostructures in fields such as quantum information.

The calculation of charge carrier states in 3D confined systems heavily depends on the geometry of the structure. In the particular case of elliptic-like QDs the analytical solution of effective mass equations is not possible in general. Furthermore, the inclusion of the effect of an externally applied electric field makes this possibility be unreachable. Therefore, numerical ways of solution for conduction and valence band states are required. In this sense, different approaches appear reported: finite- and boundary-element calculations [6, 7], variational solutions [8], and meshless schemes for the numerical solution of the effective mass equation [11, 12], to mention but a few.

It is well known that even in the case of high quality and high purity samples, semiconductor compounds contain atoms of external elements acting as impurities, not to mention the intentional doping aimed at obtaining a desired carrier concentration in the material. In consequence, the investigation of the influence of impurity atoms on the spectrum of carrier states in semiconductor-based systems

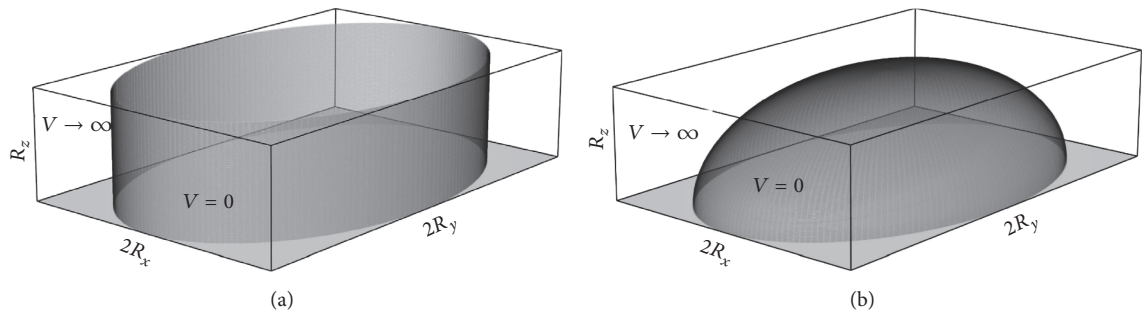

FIGURE 1: (a, b) Pictorial view of the two kinds of quantum dots considered in the present work: with constant height (a) and with variable height (b).

is always of significance. On the other hand, the optical response associated with quantum confined carrier states is an important element for both the understanding of the very energy spectrum of the systems and the design of their practical applications. In the case of elliptic-shaped systems a numerical calculation of optical transitions in InAs/GaAs QDs is reported, for example, in [6]. By using the adiabatic approximation, Gusev et al. have reported the electronic structure in low dimensional systems, with parabolic and rectangular potential, including impurity and exciton states [13, 14]. Their results are developed for quantum wells, wires, and dots, with particular spheroidal-shapes [14]. Their findings are in excellent agreement with variational calculations.

In this article we are going to present the results of a study on the electron and electron-impurity states in elliptic-shaped GaAs-based QDs, including the influence of external static electric fields. Two kinds of structures are considered, for which Figure 1 depicts their corresponding pictorial views. The calculation is carried out within the framework of the effective mass and parabolic band approximations. With the outcome information we shall discuss the light absorption related with transitions between a number of the lowest confined electron and electron-impurity states. Accordingly, the organization of the paper is as follows: Section 2 is devoted to presenting in detail the theoretical framework. Section 3 contains the obtained results and the corresponding discussions, and, finally, in Section 4 we give the conclusions.

2. Theoretical Model

Here we shall consider the motion of conduction band electrons in the 3D elliptically shaped QD under the effect of in-plane applied electric field $[\vec{F} = (F_x, F_y, 0)]$ and considering the presence of a shallow-donor impurity. The Hamiltonian of the system, within the framework of the effective mass and parabolic band approximations, is given by

$$H = -\frac{\hbar^2}{2m_{\parallel}^*}\nabla_\rho^2 - \frac{\hbar^2}{2m_{\perp}^*}\frac{\partial^2}{\partial z^2} + V(\rho, z) + |e|\,\vec{F}\cdot\vec{r} - \frac{e^2}{\varepsilon r_{ei}}. \quad (1)$$

The quantities $|e|$, $m_{\parallel}^*$ ($m_{\perp}^*$), and ε are the absolute value of the electron charge, the in-plane (growth direction) electron effective mass, and the GaAs static dielectric constant, respectively. ∇_ρ^2 is the in-plane Laplacian operator, $\vec{r} = (x, y, z)$ is the electron position, and r_{ei} is the electron-impurity distance, with the donor impurity localized at $(x_i, y_i, 0)$. Considering that the height of the structure is very small comparing with the dimensions of the base, we can use the adiabatic approximation where the 3D-confinement potential can be written as the sum between two potentials: the first one depending on the in-plane xy-dimensions and the second one depending on the z-dimension; that is, $V(\rho, z) = V_1(\rho) + V_2(z; x, y)$, where the z-dependent confinement potential ($V_2(z; x, y)$) depends of the in-plane coordinates (x, y) (in this work this dependence is associated with the variations of the height of the QD). $V_1(\rho)$ is zero into the region delimited by S_1 and infinite outside the region delimited by S_1, where S_1 is given by $x^2/R_x^2 + y^2/R_y^2 = 1$ with $z = 0$. Note that the frame of reference is localized at the gravity center of the elliptic region. Also, due to the restriction of heights with respect to the base of the dot, we take the approximation $r_{ei} \simeq |(x, y, 0) - (x_i, y_i, 0)|$ for the electron-impurity distance. This approximation does not mean changes in the calculated Coulomb correlation more than 2% with respect to the corresponding exact value.

According to the schematic view for the shape of the 3D elliptically shaped QD depicted in Figure 1, two kinds of configurations will be studied: elliptical base with constant value of the height (a) and elliptical base with elliptical dependence of the height (b).

The 3D problem in (1) does not have analytical solutions. To find the eigenfunctions and eigenvalues of the Schrödinger equation we will use the adiabatic approximation. In this paper we deal with heterostructures where the vertical dimension of the dot is small as compared with the in-plane dimensions. Under such conditions the electron has a fast-movement along the z-direction and slow-movement in the x-y plane. This is the spirit of the adiabatic approximation used in this paper where we decouple the two movements in (1). In this case we propose that the eigenfunctions of the Hamiltonian in (1) can be written as the product $\Psi(x, y, z) = N\phi(x, y)\chi(z; x, y)$, where N is the normalization constant

and $\phi(x, y)$ and $\chi(z; x, y)$ are, respectively, the eigenfunctions of the following two differential equations:

$$H_{x,y}\phi(x,y) = \left[-\frac{\hbar^2}{2m_{\parallel}^*}\nabla_\rho^2 + V_1(\rho) + |e|\,\vec{F}\cdot\vec{r} - \frac{e^2}{\varepsilon r_{ei}} + \mathfrak{E}_1(h;x,y)\right]\phi(x,y) = E\phi(x,y), \tag{2}$$

$$\left[-\frac{\hbar^2}{2m_{\perp}^*}\frac{\partial^2}{\partial z^2} + V_2(z;x,y)\right]\chi(z;x,y) = \mathfrak{E}_1(h;x,y)\cdot\chi(z;x,y), \tag{3}$$

where $\mathfrak{E}_1(h;x,y)$ is the adiabatic potential energy and corresponds to the ground state of (3) which is a function of the in-plane coordinates. It is clear that the eigenvalues and eigenfunctions of (3) are the same as those for a single quantum well with width $h(x, y)$. Three possibilities have been considered for the upper and lower surfaces (separated by the distance $h(x, y)$) in Figure 1: (i) a QW with two rigid potential barriers, (ii) a symmetric QW with finite potential barriers (V_0), and (iii) an asymmetric structure with infinite and finite (V_0) barriers. In the first case the adiabatic potential is given by

$$\mathfrak{E}_1(h;x,y) = \frac{\hbar^2\pi^2}{\left[2m_{\perp}^* h(x,y)^2\right]} \tag{4}$$

whereas in the second and third cases, respectively, it is obtained by the first solution of the transcendental equations

$$\tan\left[\frac{h(x,y)\beta}{2}\right] - \frac{\xi}{\beta} = 0, \qquad \cot\left[h(x,y)\beta\right] + \frac{\xi}{\beta} = 0, \tag{5}$$

where $\xi = \sqrt{(2m_{\perp,B}^*/\hbar^2)[V_0 - \mathfrak{E}_1(h;x,y)]}$, $\beta = \sqrt{(2m_{\perp,W}^*/\hbar^2)\mathfrak{E}_1(h;x,y)}$, and $m_{\perp,W}^*$ ($m_{\perp,B}^*$) refers to the effective mass inside (outside) the dot region.

The energy V_0 is equal to the barrier potential for electrons in GaAs surrounded by a Ga_{1-x} Al_xAs material. $V_0 = Q\Delta E_g$, where Q is the band offset and ΔE_g is the gap difference between the Ga_{1-x} Al_xAs and GaAs materials; here we take $Q = 0.6$ and $\Delta E_g = (1155x + 370x^2)$ meV and $x = 0.3$ for the aluminum concentration.

The eigenfunctions and eigenvalues of (2) can be obtained by several methods. In this work, particularly, we have used two different methods to confirm our findings: (i) expansion of the wave function in a set of complete wave functions associated with a confined electron in a square rectangular box (with dimensions $L_x \times L_y$) with infinite confinement potential [18–21] and (ii) the finite elements method (FEM). In the first case, we have chosen to approach the solution of the in-plane problem in (2) by means of the following 2D expansion [18–21]:

$$\phi(x,y) = \frac{2}{\sqrt{L_x L_y}}\sum_{n,m} C_{n,m}\sin\left[\frac{n\pi(x + L_x/2)}{L_x}\right]\cdot\sin\left[\frac{m\pi(y + L_y/2)}{L_y}\right]. \tag{6}$$

This means that we are writing the eigenfunctions of the in-plane problem as a linear combination of the independent solutions of a rectangular quantum box with infinite potential barriers. For a more realistic approximation, the dimensions L_x and L_y must be chosen appropriately larger than the typical in-plane ellipse-size. The calculation procedure then implies the construction of a Hamiltonian matrix from $H_{x,y}$ and its subsequent diagonalization in order to obtain the eigenenergies E_j and the set of expansion coefficients $C_{n,m}^{(j)}$ that describe the allowed quantum states.

In this study we have used a basis of sine functions in a region $L_x = L_y = 5a_0$ with quantum numbers n and m both running from 1 to 50, which gives us a total of 2500 functions. The resulting set of states is sorted out in increasing order of energy and after that we proceeded to choose the first $N = 200$ states to diagonalize the Hamiltonian. With that choice we obtained a convergence of the lowest ten energy states up to $0.05R_0$ for the highest fifteen states (where $R_0 = \hbar^2/2m_{\parallel}^* a_0^2$ is the effective unit for energy, $a_0 = \hbar^2\varepsilon/m_{\parallel}^* e^2$ being the effective unit for length). Calculations were made also for $L_x = L_y = 10a_0$ with $N = 300$ and for $L_x = L_y = 7a_0$ with $N = 700$ and the obtained set of the lowest fifteen energies did not change more than $0.05R_0$. Also the condition $L_x = L_y = 10a_0$ with $N = 700$ was studied with the same convergence.

With the aim of solving the eigenvalues problem given by (2) by means of FEM, we introduce the *Sobolev Space* $H_0^1(S_1)$, which is formed by functions u, such that u and ∇u are defined and square-integrable functions on S_1. We consider the variational form for (2) in S_1 joined with a homogeneous Dirichlet boundary condition, which arises from considering infinity confinement outside S_1: Find $\phi \in H_0^1(S_1)$ and $E \in \mathbb{R}$ such that, for any test function $\psi \in H_0^1(S_1)$, (7) is satisfied. Numerical solutions of this problem were obtained using solvers implemented in *FreeFem++* [22].

$$\int_{S_1}\left[\frac{\hbar^2}{2m_{\parallel}^*}\nabla\phi\cdot\nabla\psi + \left(V_1(\rho) + |e|\,\vec{F}\cdot\vec{r} + \mathfrak{E}_1(h;x,y)\right)\cdot\phi(x,y)\,\psi(x,y)\right]dx\,dy = E\int_{S_1}\phi(x,y)\cdot\psi(x,y)\,dx\,dy. \tag{7}$$

To use the FEM we have defined three contour lines: (i) S_1-boundary, with 300 points, which corresponds to the xy-boundary region of the QD, (ii) an auxiliary circular boundary to define the maximum variation of the Coulomb

interaction, centered at the impurity position with radius $0.2a_0$ and 30 points, and (iii) a second auxiliary circular boundary, also centered at the impurity position, enclosing an empty space with radius $10^{-4}a_0$, to prevent the singularity associated with the Coulomb interaction. Note that these two auxiliary boundaries were chosen so as to converge to the 2D-hydrogenic binding energy ($4R_0$) for large enough dimensions of the elliptical region.

The knowledge of the wave functions $\Psi_j(x, y, z)$ and their corresponding energy values is crucial to the study of the optical response related with interstate electron transitions in the QD. We have chosen to investigate the optical absorption coefficient, which is derived from the imaginary part of the dielectric susceptibility that characterizes the electric polarization of the electron system under the influence of the electric field of an electromagnetic signal of frequency ω [23, 24]. The working expression for the optical absorption coefficient is

$$\alpha(\omega) = \sum_{l>j=1}^{4} \omega \sqrt{\frac{\mu_0}{\varepsilon\epsilon_0}} \frac{\left|M_{jl}\right|^2 e^2 \rho_{jl} \hbar\Gamma_{jl}}{\left(E_{jl} - \hbar\omega\right)^2 + \left(\hbar\Gamma_{jl}\right)^2}, \tag{8}$$

where the quantity $E_{jl} = E_l - E_j$ is the energy difference associated with the transition between an initial state with energy E_j and a final state E_l. M_{jl} is the electric dipole moment off-diagonal matrix element involving those very states (in this work calculations are for circular xy-polarization of the incident radiation), whereas Γ_{jl} are the corresponding transition damping rates. The quantities μ_0 and ϵ_0 are the free space magnetic permeability and dielectric permittivity. Finally, $\rho_{jl} = 2(f_j - f_l)/V$ is the corresponding three-dimensional electron concentration [23], where

$$f_r = \frac{1}{1 + \exp\left[\left(E_r - E_F\right)/k_B T\right]} \tag{9}$$

is the Fermi-Dirac occupation number (E_F is the Fermi level energy, V is the system's volume, and T is the temperature).

The input parameters for a prototypical GaAs QD are as follows: $\varepsilon = 12.35$, $c = 3 \times 10^8$ m/s, $\epsilon_0 = 8.85 \times 10^{-12}$ F/m, $\mu_0 = 1.256 \times 10^{-6}$ T m/A, $e = 1.6 \times 10^{-19}$ C, and $m_e^* = 0.067m_0$, where m_0 is the free electron mass. In GaAs we deal with spherical-symmetric conduction effective mass; that is, $m_\parallel^* = m_\perp^* = m^*$. Calculations are for $m^* = 0.067m_0$ in the GaAs region and $m^* = 0.086m_0$ in the $Ga_{0.7}Al_{0.3}As$ barriers when the finite confinement is considered. Here m_0 is the free electron mass. For the length and energy effective units the considered values are, respectively, $a_0 = 97.98$ Å and $R_0 = 9.95$ meV. For the broadening we took the value $\Omega_{jl} = \hbar\Gamma_{jl} = 3$ meV [25, 26], in agreement with the corresponding value determined experimentally and supported by theoretical calculations [27] for a structure similar to ours. The broadening obviously depends on the temperature, dimensions, roughness, doping concentration, alloy disorder, and nonparabolicity of subbands, as well as the influence of elastic and inelastic scattering mechanisms. We did not take into account these dependencies in our calculations and, for that reason, we justify our choice for the broadening parameter due to the very good resolution obtained for the main structures in the absorption coefficient.

3. Results and Discussion

Figure 2 shows the functional dependence of the energy of lowest confined states with regard to the change in the horizontal semilength for the case of the elliptical quantum dot with constant height depicted in Figure 1(a). The results are for zero applied field and correspond to two different values of the semilength R_y. The upper row corresponds to conduction band states [graphics (a) and (b)], and the lower row contains the energies of electrons coupled to the donor impurity located at the elliptical QD center. As can be expected, the increase of the QD size implies the reduction of the allowed confined energy values due to the loss in carrier localization. The inclusion of the Coulombic center (donor impurity) leads to an additional decrement of the energies as a result of the attractive electron-impurity interaction. Although the calculation was performed using the FEM in all cases, the spectral scheme that involves the diagonalization of the Hamiltonian matrix resulting from expansion (6) was also applied and the corresponding results appear superimposed to the FEM ones in Figure 2(a), showing a remarkably good coincidence. Note that in both cases of the numerical calculations the confinement potential around the elliptical region is infinite.

In Figure 2(c) we have also included the electron-impurity correlated energy for the ground state calculated via a variational technique and considering the 3D-shape of the structure (it means considering the 3D-character of the electron-impurity distance) [15–17]. Calculations were done with a one-variational parameter trial wave function. As can be seen, the FEM-results and the variational calculations agree with differences less than 2%, as was established above after (1).

In Figure 3 we are presenting the lowest electron-impurity energies, depending on the position of the donor impurity atom along the y-axis [cases (a) and (c)] and the x-axis [cases (b) and (d)] for the QD system of Figure 1(a). The static electric field is absent in cases (a) and (b). At the same time, a static electric field of 100 kV/cm is assumed to be applied along the y-direction [case (c)] and along the x-direction [case (d)]. The zero-field configurations show a symmetric dependence of the coupled electron-impurity energies which, depending on the symmetries of the unconnected conduction band electron states, will show maxima and minima at different donor impurity positions. For all depicted level is coincident if the donor atom is placed at one of the QD borders the effect of the electron-impurity attraction is weaker and therefore the energy levels tend to go up (this is due to the an infinite barrier effect). It is worth noticing the presence of level anticrossings, typical of nonisotropic 2D or 3D systems.

Including the influence of the static electric field modifies the above-mentioned picture. This time the electron density of probability becomes displaced inside the QD region. As a consequence, depending on the localization of the donor impurity, the energy values will be shifted upwards or downwards. This is a consequence of the rise or the fall of the expected electron-impurity distance, respectively, implying the weakening or the strengthening of the attractive

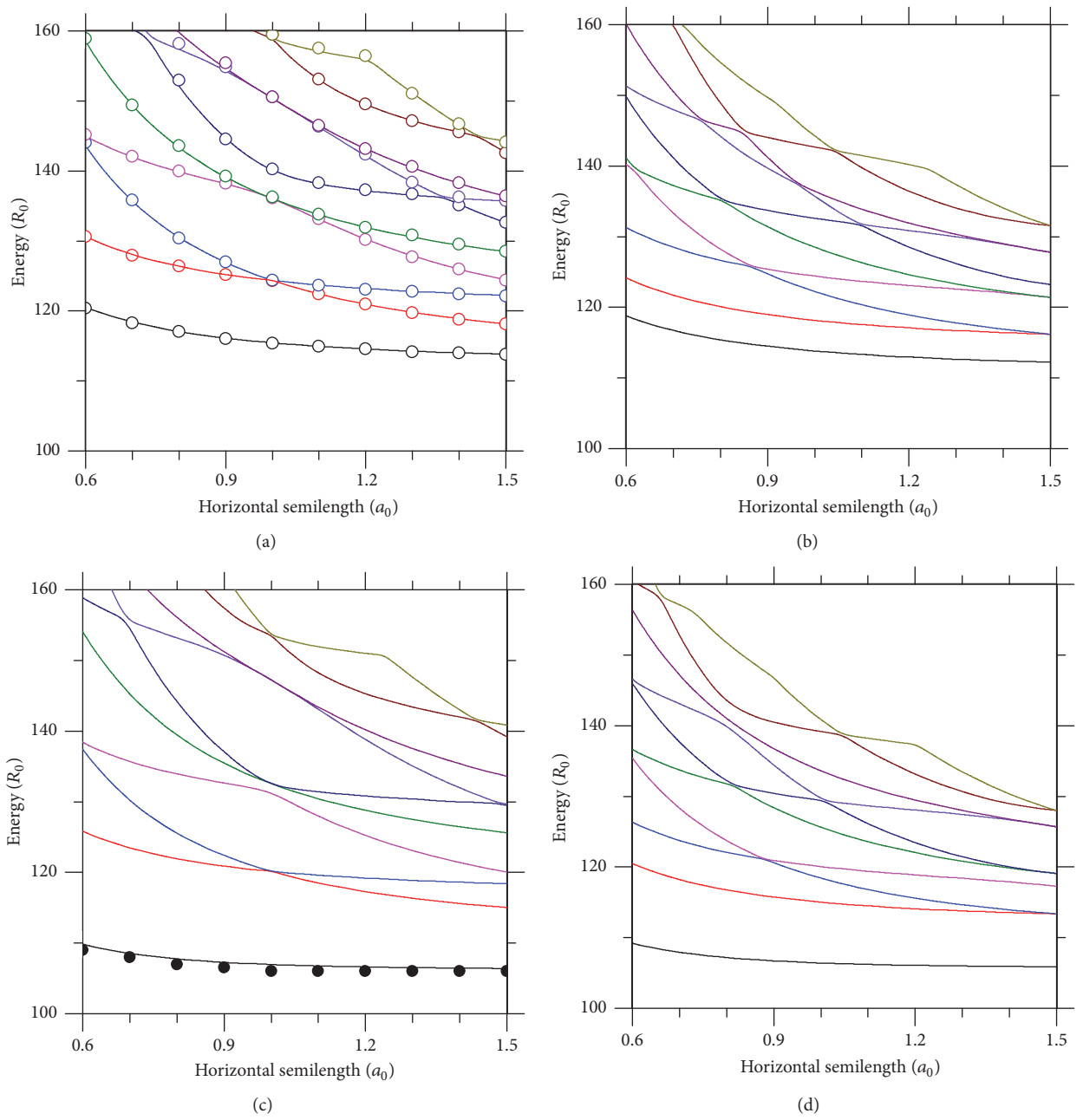

FIGURE 2: (a, b) Energy of the first ten confined-electron states in an elliptical GaAs quantum dot as a function of the horizontal semilength (R_x) of the structure for two different values of the vertical length R_y: $1.0a_0$ (a) and $1.5a_0$ (b). In (c) and (d) the corresponding results including the effects of on-center donor impurity are depicted. The results are for zero electric field. A constant dot-height of $0.3a_0$ has been considered. In (a) the open symbols correspond to calculations using a diagonalization method. In (c) the full symbols correspond to theoretical calculations considering the 3D-character of the electron-impurity distance and using a variational procedure [15–17].

Coulombic interaction. The field effect is more pronounced when it is applied along the horizontal direction of the elliptical cross section because in that case the field-induced electron delocalization is stronger. It can be seen that the electric field causes the appearance of level anticrossings in cases not appearing when $F = 0$. This is another consequence of the field-induced additional symmetry loss.

These features can be confirmed by observing the evolution of the lowest electron confined energy levels as functions of the electric field strength shown in Figure 4. Again, we are dealing with the constant height elliptic-shaped disc geometry and the dimensions R_x and R_y are fixed. Upper row [cases (a) and (b)] corresponds to the conduction band states in absence of impurity and the graphics in lower row [cases (c) and (d)] contain the results that include the donor center atom in the structure. The decrease of the energy level position as a result of the increment in the field intensity (greater loss in electron localization) is readily apparent in

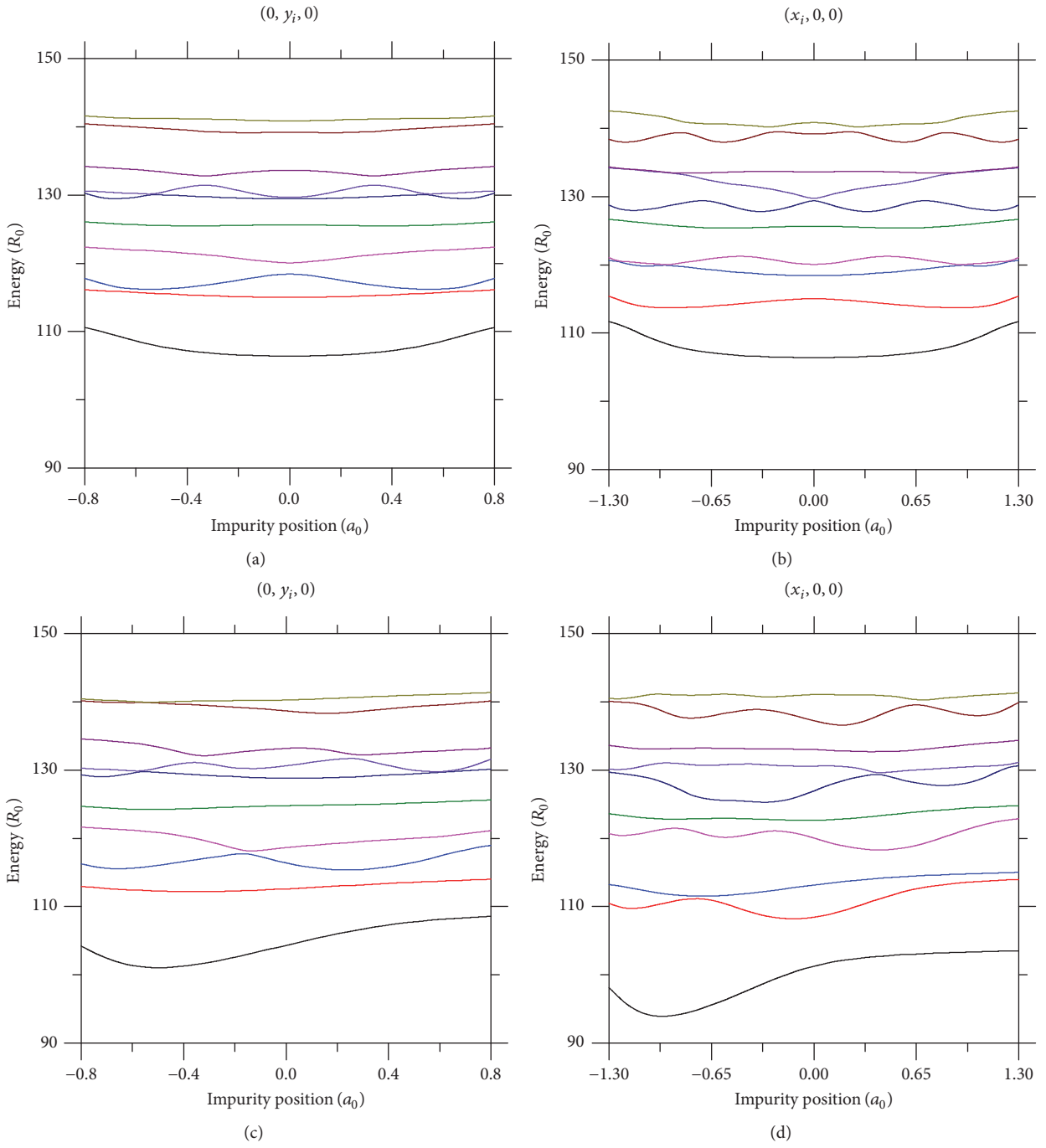

Figure 3: (a, b) Energy of the first ten confined-electron states in an elliptical GaAs quantum dot as a function of the impurity position along the y-direction (a, c) and x-direction (b, d). The results are for $R_x = 1.5a_0$ and $R_y = 1.0a_0$ for zero applied electric field (a, b), $F = (0, 100, 0)$ kV/cm (c), and $F = (100, 0, 0)$ kV/cm (d). A constant dot-height of $0.3a_0$ has been considered.

all cases. The above discussed situation where the presence of the attractive electron-impurity interaction implies the larger rate of decrement is also clearly present. Furthermore, the more noticeable effect of the x-oriented electric field is observed as well.

The results for the variation of the energy levels as functions of R_x in the case of the variable height QD [see Figure 1(b)] is shown in Figure 5. There, the zero-field situation is explored for two different geometrical configurations. In one of them, the QD height is assumed to vary in the form $h = R_z\sqrt{1 - x^2/R_x^2 - y^2/R_y^2}$ [cases (a) and (c)]. In the second one, the height changes according to $h = h_0 + R_z\sqrt{1 - x^2/R_x^2 - y^2/R_y^2}$ [cases (b) and (d)]. This means that close to the QD bottom there is a strip of constant height, resembling the presence of a possible wetting layer.

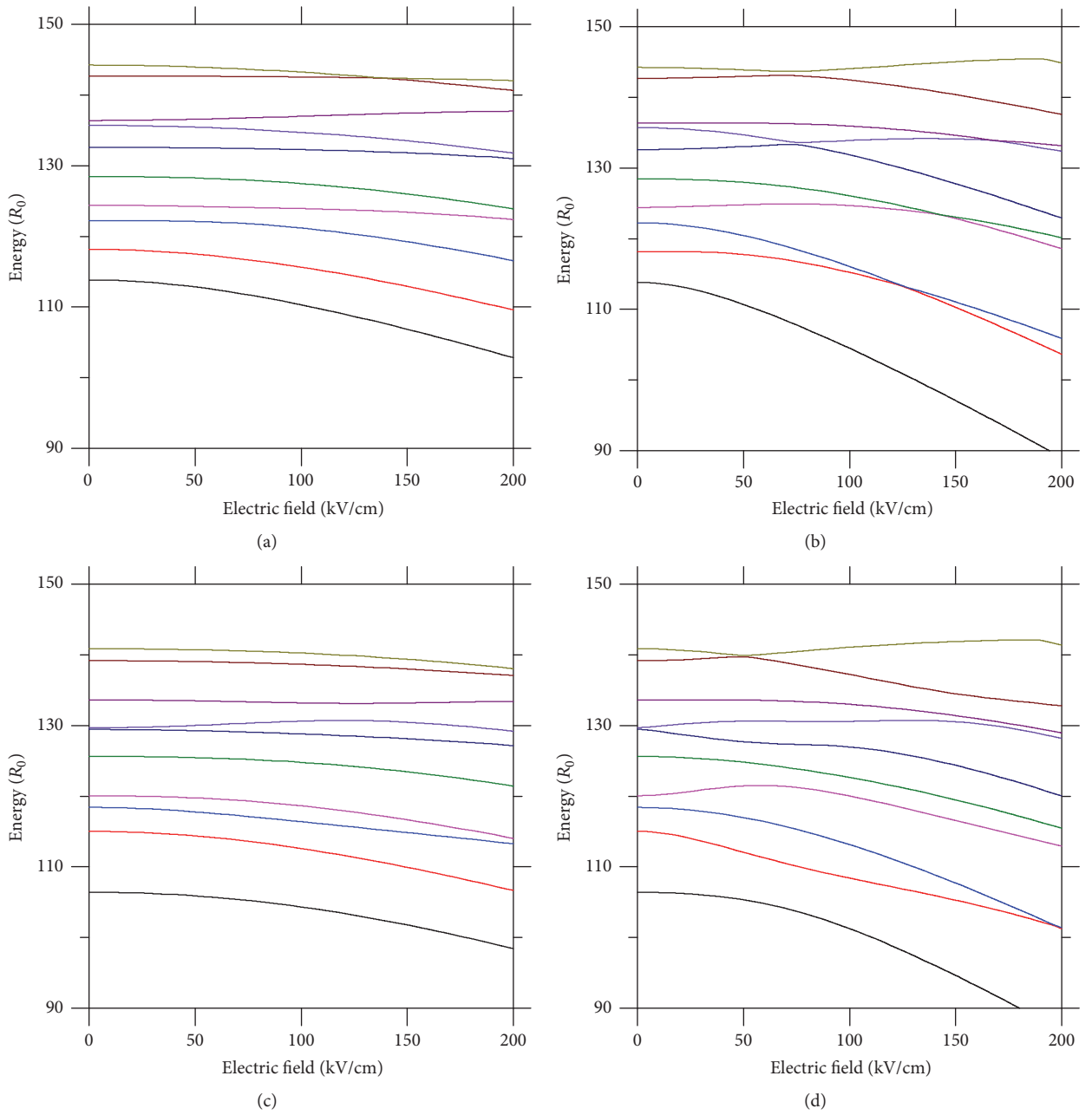

FIGURE 4: (a, b) Energy of the first ten confined-electron states in an elliptical GaAs quantum dot as a function of the applied electric field along the y-direction (a, c) and x-direction (b, d). The results are for $R_x = 1.5a_0$ and $R_y = 1.0a_0$ without impurity (a, b) and with on-center impurity (c, d). A constant dot-height of $0.3a_0$ has been considered.

In addition, the presence of the donor impurity center is included in the results appearing in Figures 5(c) and 5(d).

The reduction in the energy values as a consequence of the increase in the horizontal dot size, as discussed above in the constant height case, is observed as well. It is interesting to note that the inclusion of a nonzero-height strip at the base of the QD that amounts 33% of increase in the top height causes a significant redshift of the confined energies. For instance, in the case of the ground state, the energy decreases approximately 40% with respect to the unstriped geometry, both with and without the presence of the impurity atoms. The presence of anticrossings is preserved.

In Section 2 we have commented the possibility of the numerical calculation of the confined states in the QD which has the elliptical-shaped configuration with the finite confinement potential via FEM. Accordingly, Figure 6 contains the zero electric field results for the variation of the confined states in the case of nonconstant height geometry [analogous to that appearing in Figure 1(b)] as functions of R_x. Graphics (a) and (b) correspond to conduction band electron states without impurity effect, whereas graphics (c)

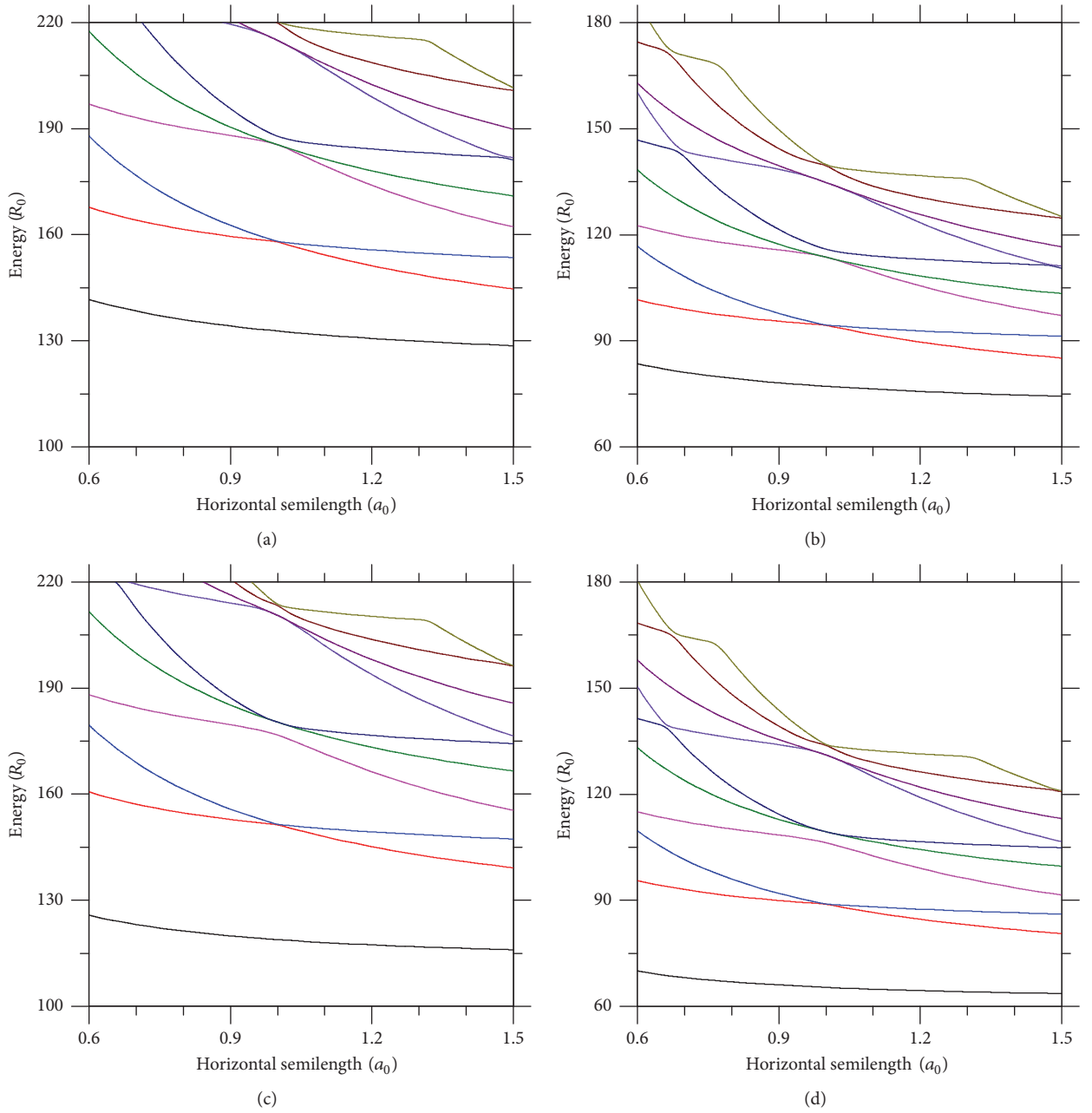

FIGURE 5: (a, b) The results are as in Figure 2, but here we are interested in an quantum dot with variable height. In (a, c) the height of the dot is given by $h = R_z\sqrt{1 - x^2/R_x^2 - y^2/R_y^2}$, whereas in (b, d) the results are for $h = h_0 + R_z\sqrt{1 - x^2/R_x^2 - y^2/R_y^2}$. Calculations are for $R_y = 1.0a_0$, $R_z = 0.3a_0$, and $h_0 = 0.1a_0$.

and (d) show the allowed electron-donor impurity energies. The configurations chosen for the finite potential energy confinement profiles are as follows: (i) With QD height given by $h = R_z\sqrt{1 - x^2/R_x^2 - y^2/R_y^2}$ [cases (a) and (c)], the quantum well along the z-direction is taken as symmetric finite barrier one with depth provided by the corresponding band offset of the $Al_{0.3}Ga_{0.7}As/GaAs$ system. (ii) With QD height given by $h = h_0 + R_z\sqrt{1 - x^2/R_x^2 - y^2/R_y^2}$, with $h_0 = 0.25a_0$ [cases (b) and (d)], the quantum well along the z-direction has a bottom finite barrier and an infinite barrier at the top that could simulate an upper free-standing configuration.

In first place one may readily noticed that, as it should be expected, the values of the obtained energies are significantly smaller compared with the previously discussed infinite potential barrier cases. However, the behavior of the energies as functions of the horizontal semilength are qualitatively similar, with the same arguments related with the electron spatial localization and the expected electron-impurity distance as the key elements for their explanation. It should be kept in mind that the confining configuration (ii)

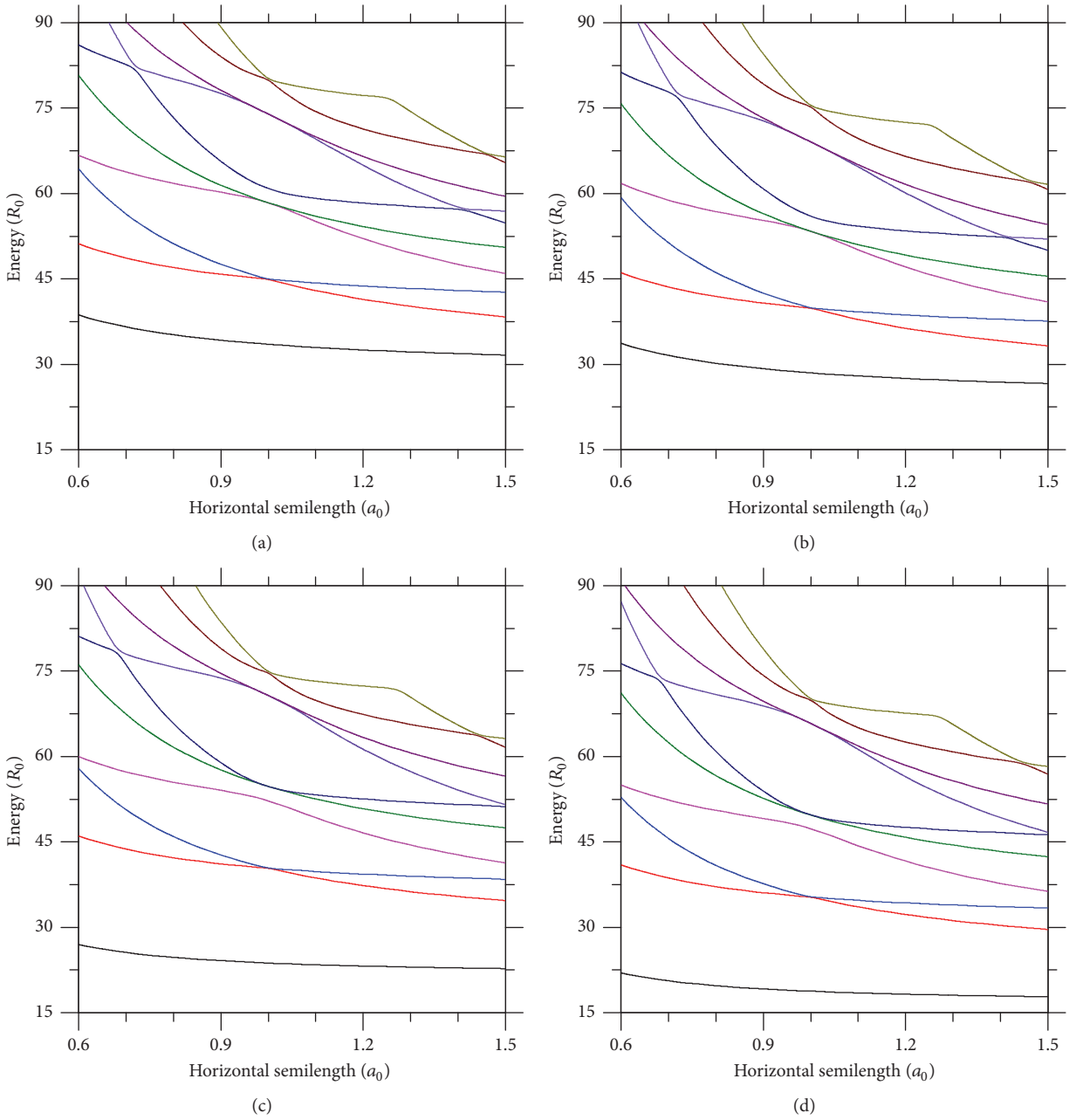

FIGURE 6: (a, b) The results are as in Figure 2, but here we are dealing with a variable height of the dot. In (a, c) the height of the dot is given by $h = R_z\sqrt{1 - x^2/R_x^2 - y^2/R_y^2}$ with symmetric finite confinement potentials along the z-direction, whereas in (b, d) the results are for $h = h_0 + R_z\sqrt{1 - x^2/R_x^2 - y^2/R_y^2}$ with asymmetric finite-infinite-confinement potentials along the z-direction. Calculations are for $R_y = 1.0a_0$, $R_z = 0.3a_0$, and $h_0 = 0.25a_0$.

implies a larger size of the width of the quantum well along the vertical direction. As a consequence, in spite of the presence of a top infinite barrier, the obtained energies are lower in both the uncoupled and Coulombic-coupled situations.

In order to proceed with the investigation of the optical absorption coefficient in the elliptic-shaped QDs we need to evaluate the off-diagonal electric dipole matrix elements associated with the interstate transitions that will be considered. As indicated in (8), only the contributions coming from the transitions that involve the lowest four confined states shall be included. Following the same geometrical, compositional, and interaction setups that led to the energy level results in Figures 2–6, the corresponding variations of the M_{ij} are displayed in Figures 7–11, respectively. Note that all the results presented in Figures 7–11 are for the low temperature regime (4 K).

The different, and sometimes jumbled, behaviors of these quantities are governed by two main elements: the spatial

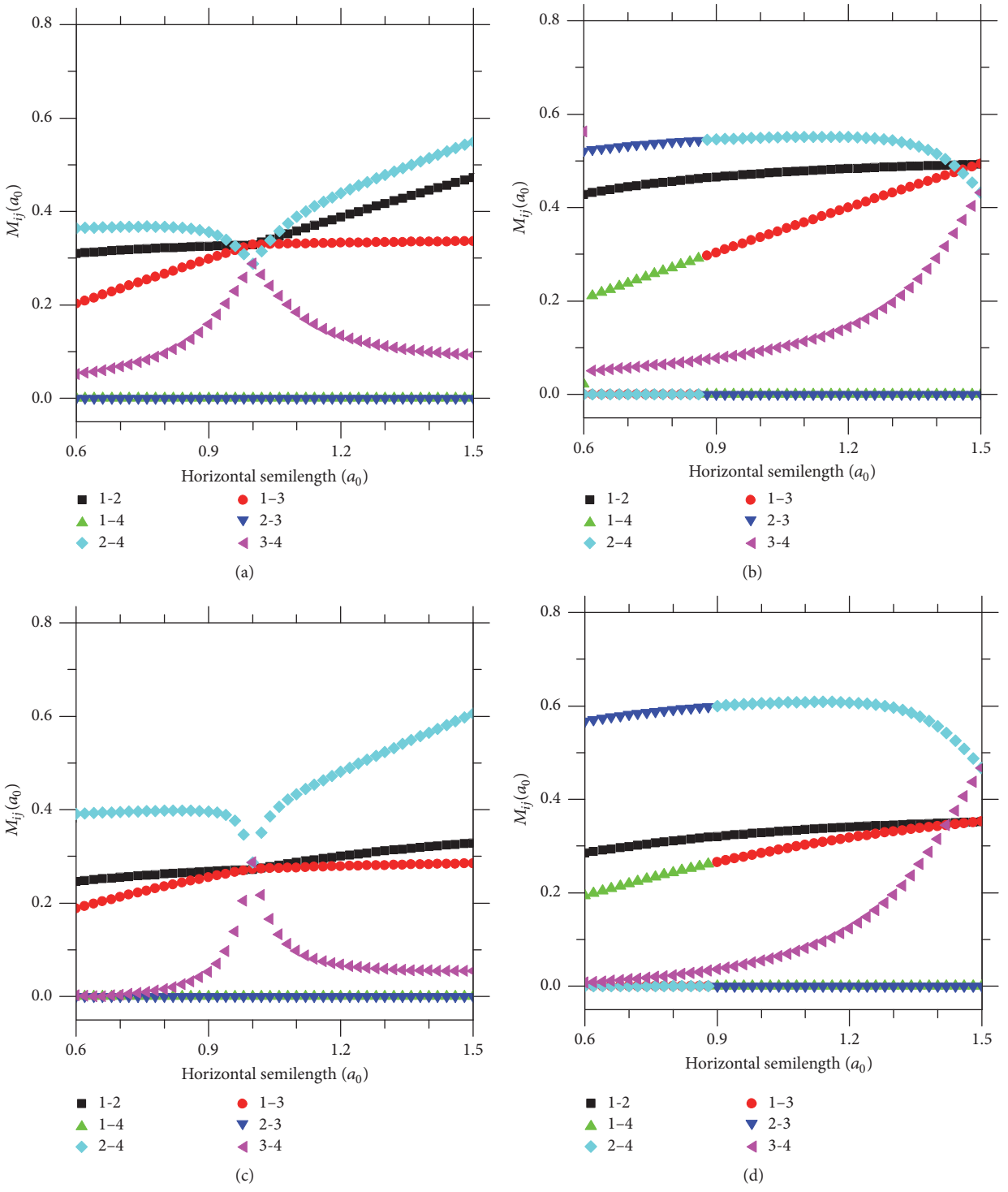

FIGURE 7: Dipole matrix elements for circular polarization of the incident radiation considering combinations between the first four confined states. The results are obtained under the same geometrical, compositional, and interaction configurations leading to Figure 2.

extension and the symmetry of the involved wave functions. They, combined with the polarization of the incident light (here considered to be circular), determine whether the dipole matrix element vanishes or remains finite as well as its functional dependence with respect to the varying quantity in the system. For instance, the effect of the anticrossings, which imply the sudden change in the symmetry of certain wave function and, therefore, the imposition of a particular selection rule for the transition under specific circumstances, can be clearly noticed.

The total light absorption coefficient that includes the contribution of the above transitions commented on is shown

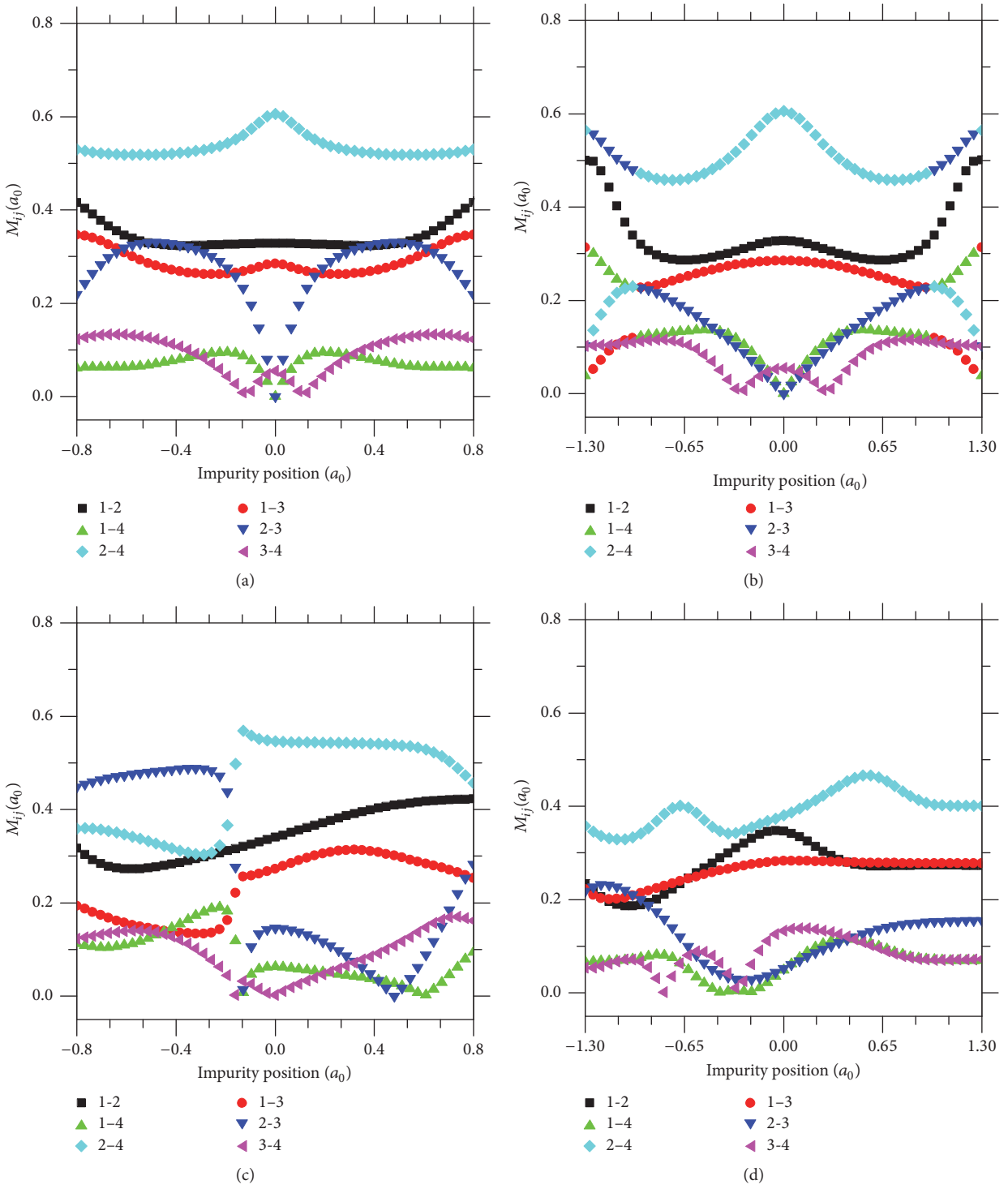

FIGURE 8: Dipole matrix elements for circular polarization of the incident radiation considering combinations between the first four confined states. The results are obtained under the same geometrical, compositional, and interaction configurations leading to Figure 3.

in Figure 12 as a function of the incident photon energy for two different values of the temperature $T = 4$ K [(a), (c)] and $T = 300$ [(b), (d)]. The geometry is that with constant height, depicted in Figure 1(a), with fixed dimensions. The electric field, oriented along the y-direction, intensity is varied from 8 kV/cm to 200 kV/cm. Graphics (a) and (b) correspond to the case without the presence of the impurity atom, and in the graphics (c) and (d) the system with on-center donor impurity atom is taken into account. In the case without impurity we can identify the resonant peaks associated with

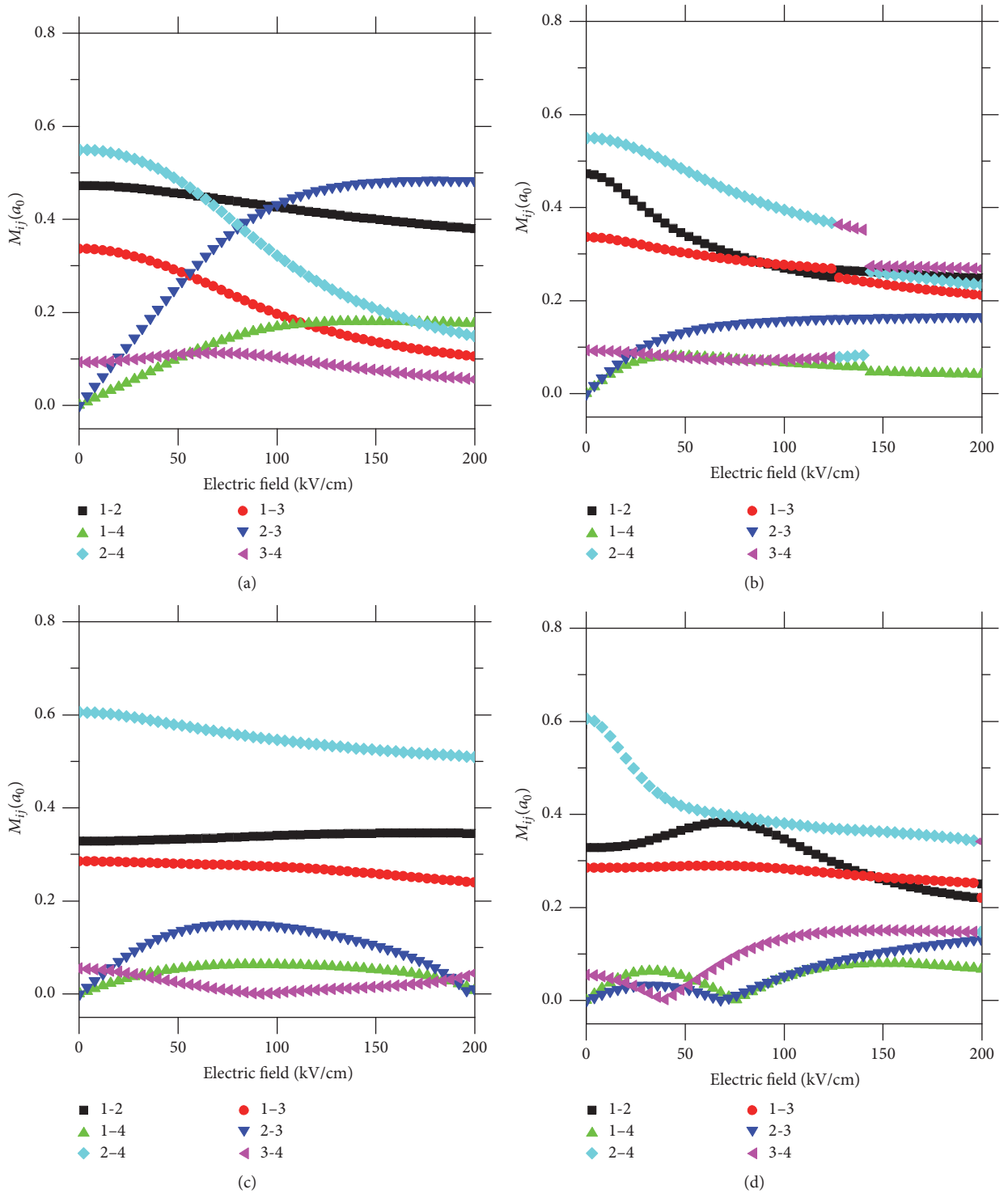

FIGURE 9: Dipole matrix elements for circular polarization of the incident radiation considering combinations between the first four confined states. The results are obtained under the same geometrical, compositional, and interaction configurations leading to Figure 4.

transitions having the ground state as the initial one. The shift of the peaks as a result of the increment in F can be identified by observing the behavior of the involved state energies as functions of the electric field strength in Figure 4. The evolution of the resonant peak amplitudes can also be noticed which follow the dependence generated by the combined effects of the variation of the resonant peak position and the electric dipole moment matrix element through the product $E_{ij}|M_{ij}|^2/\hbar$.

In our calculation, the effect of the temperature is supposed to fall on the population of the transition states. We are assuming that the influence of T on the transition energy

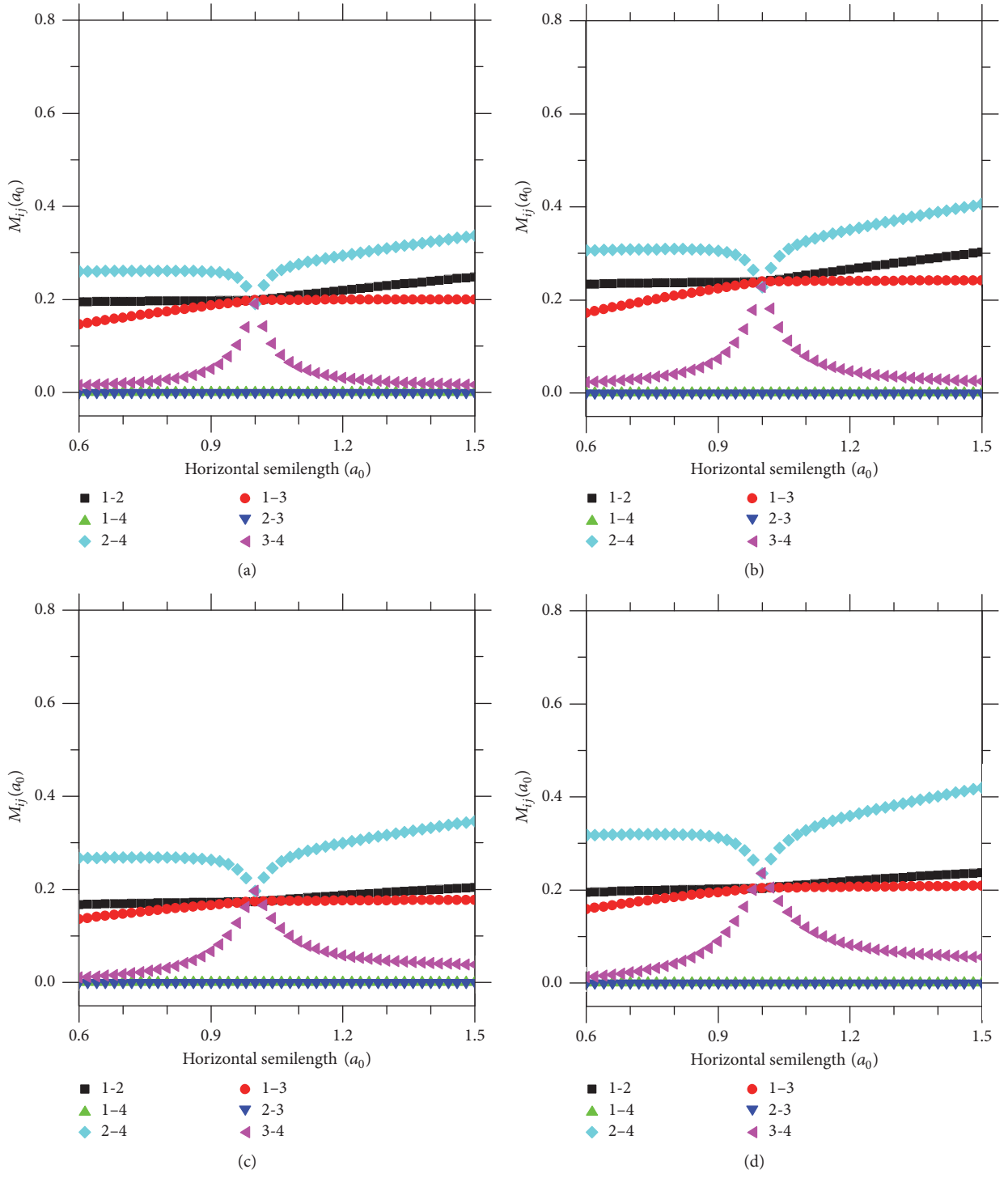

FIGURE 10: Dipole matrix elements for circular polarization of the incident radiation considering combinations between the first four confined states. The results are obtained under the same geometrical, compositional, and interaction configurations leading to Figure 5.

differences and state wave functions is not significant and can be neglected. Note that in the case of finite quantum wells in the z-direction, the temperature coefficient of the gap for the well and barrier materials is the same and consequently there is no change with temperature of the height of the confinement potential. In the case of the effects of the temperature on the electron effective mass and static dielectric constant, they are global and involve almost rigid modifications on the whole spectra without changes in the transition energies. Accordingly, the results depicted in Figures 12(b) and 12(d) reveal the consequence of the change in the level populations, with the appearance of absorption

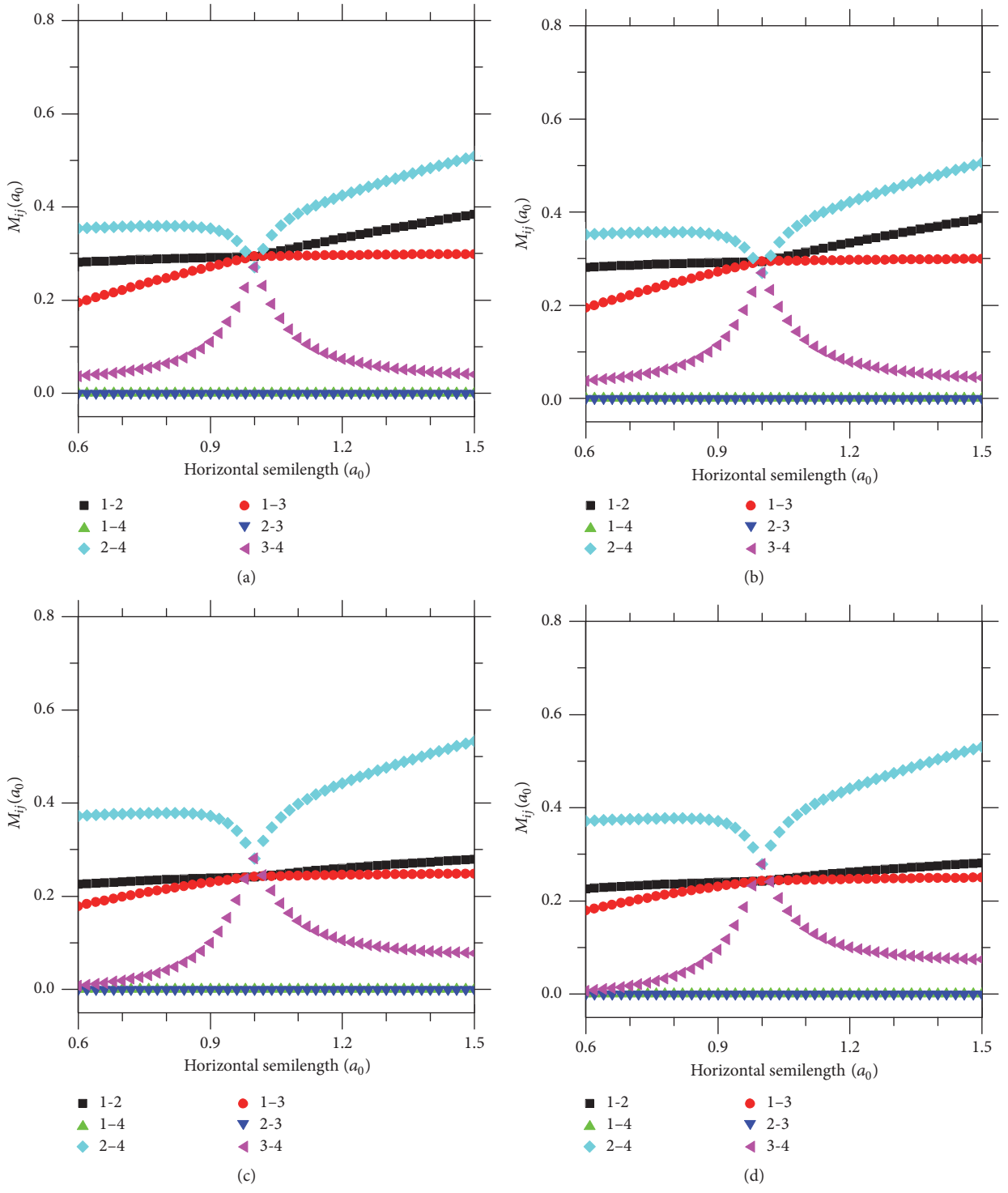

FIGURE 11: Dipole matrix elements for circular polarization of the incident radiation considering combinations between the first four confined states. The results are obtained under the same geometrical, compositional, and interaction configurations leading to Figure 6.

peaks for $T = 300$ K, additional to those observed at low temperature. At the same time, the variation in ρ_{ij} conditions the change in the resonant peak amplitudes as can be noticed.

Finally, Figure 13 shows the calculated total optical absorption coefficient in the symmetric finite confinement configuration of the elliptic-shaped QD with nonconstant height. The light absorption coefficient is presented as a function of the incident photon energy and curves are drawn taking the horizontal elliptic size R_x as a parameter, with R_y and R_z fixed. Again, two values of the temperature are taken

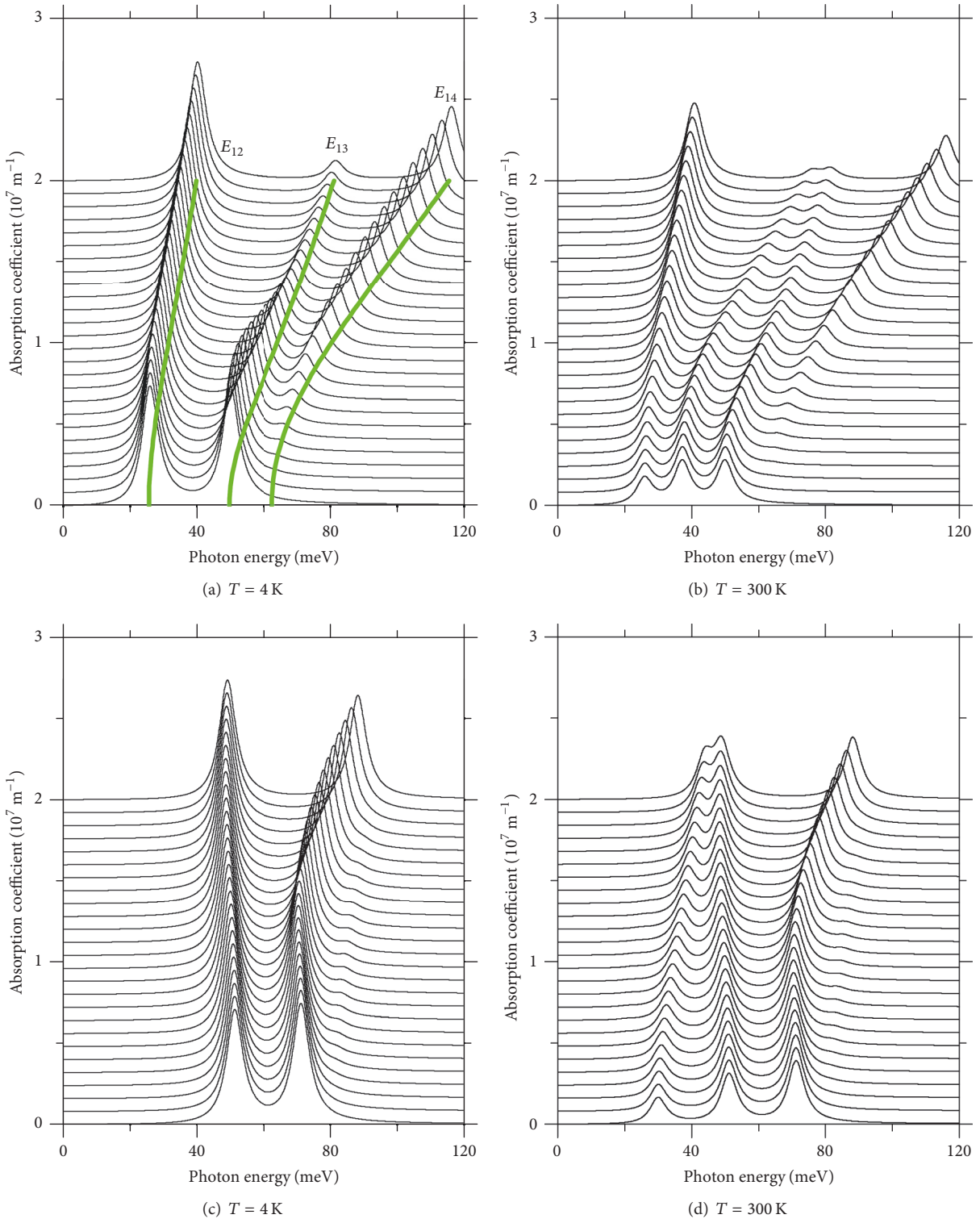

FIGURE 12: Total absorption coefficient as a function of the incident photon energy for several values of the electric field applied in the y-direction and varying in steps of 8 kV/cm from 0 to 200 kV/cm. $R_x = 1.5a_0$, $R_y = 1.0a_0$, and constant dot-height of $0.3a_0$. The curves are shifted 0.8×10^7 m^{-1}. In (a) and (b) the results are without donor impurity whereas in (c) and (d) they are for on-center impurity. Two values of temperature have been considered as indicated in the figures. The green lines correspond to the calculated energy transitions from Figure 4(a).

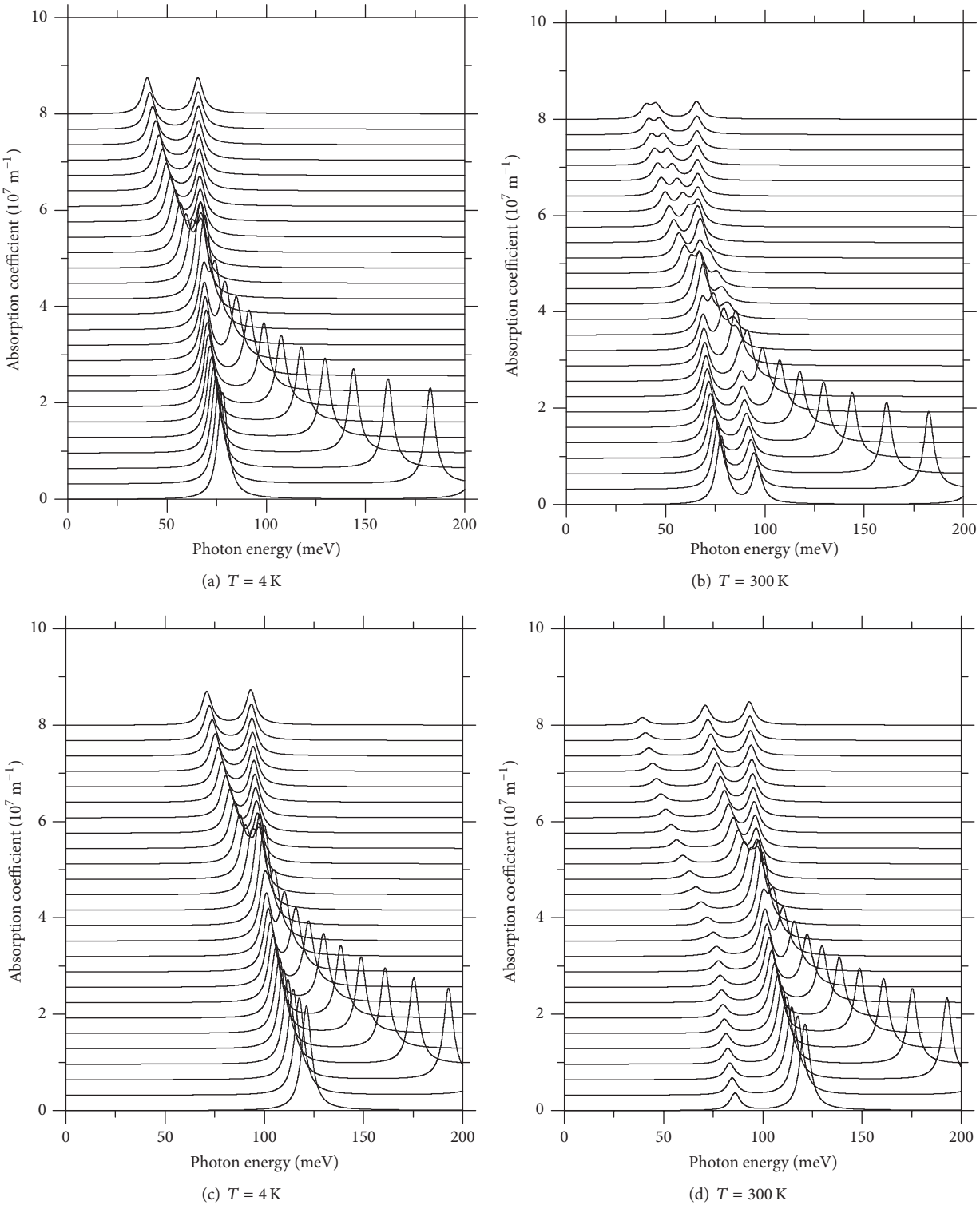

FIGURE 13: Total absorption coefficient as a function of the incident photon energy for several values of the horizontal length varying in steps of $0.04a_0$ from $0.5a_0$ to $1.5a_0$. The curves are shifted 3.2×10^7 m^{-1}. The height of the dot is given by $h = R_z\sqrt{1 - x^2/R_x^2 - y^2/R_y^2}$ with symmetric finite confinement potentials along the z-direction. Calculations are for $R_y = 1.0a_0$ and $R_z = 0.3a_0$. In (a) and (b) the results are without donor impurity whereas in (c) and (d) they are for on-center impurity. Two values of temperature have been considered as indicated in the figures.

into account. Graphics of the results without the presence of any impurity are labeled (a) and (b), whilst (c) and (d) correspond to the case with an on-center ionized donor atom.

The shifts of the resonant absorption peak positions can be explained as above, that is, by observing the behavior of the confined state energies appearing in Figures 6(a) and 6(c) and the variation of the differences between them. The change in their amplitudes is, once again, justified by the behavior of the involved transition energies and the electric dipole matrix elements shown in Figures 11(a) and 11(c). Also, as we previously commented, the influence of a higher temperature, affecting the electron concentration ρ, allows for the resolution of other transition peaks, highlighting the thermal effect in this case.

4. Conclusions

In the present work we have addressed the calculation of the conduction band effective mass states of elliptically shaped quantum dots with finite and infinite confinement potentials, the presence of a donor impurity atom, and the influence of externally applied static electric fields. The solution of the Schrödinger-like effective mass differential equation incorporates the adiabatic approximation to uncouple the electron motion along the z and (x, y) directions, as well as the finite element method to solve the resulting differential problem. The use of the finite element method using *FreeFem++* is an important tool for solving this kind of problem. Results also were obtained via a spectral procedure which reveals a very good agreement with the finite element scheme.

Our results confirm the known effects of the presence of the electron-impurity interaction and the application of static electric fields on the spectrum of carrier confined in quantum nanostructures, indeed with the particularities associated with the specific geometry of the system under study.

The light absorption associated with electron transitions between the allowed quantum states in each case is studied making use of the previously calculated energies and wave functions. It is shown that the changes in the electron state energies and probability densities due to modifications in the type of confinement, the geometry, and the presence or absence of the donor impurity center, as well as the variation of the level population with temperature, are all causes for the shift of the absorption resonant peaks and/or the increment or reduction of their corresponding amplitudes.

Quantum dots with the shape here discussed are, actually, experimentally realized systems, with well-identified current and prospective applications. We hope, with this work, to shed some light on the electronic and optical features of a GaAs-based structure of this type.

Conflicts of Interest

The authors declare that they have no conflicts of interest.

Acknowledgments

This research is funded by Vietnam National Foundation for Science and Technology Development (NAFOSTED) under Grant no. 103.01-2015.93. The authors are grateful to the Colombian Agencies CODI-Universidad de Antioquia (Estrategia de Sostenibilidad de la Universidad de Antioquia) and Facultad de Ciencias Exactas y Naturales-Universidad de Antioquia (C. A. Duque and A. L. Morales Exclusive Dedication Projects 2016-2017). M. A. Londoño is grateful to Colciencias-Ecopetrol for financial support through the project *Migración Sísmica Pre-Apilado en Profundidad por Extrapolación de Campos de Onda Utilizando Computación de Alto Desempeño para Datos Masivos en Zonas Complejas* (Code 111553130555).

References

[1] L. C. Lew Yan Voon and M. Willatzen, "On triaxial ellipsoidal quantum dots," *Journal of Physics: Condensed Matter*, vol. 16, no. 7, article 1087, 2004.

[2] B. Szafran, F. M. Peeters, S. Bednarek, and J. Adamowski, "Anisotropic quantum dots: correspondence between quantum and classical Wigner molecules, parity symmetry, and broken-symmetry states," *Physical Review B—Condensed Matter and Materials Physics*, vol. 69, no. 12, Article ID 125344, 2004.

[3] K. G. Dvoyan, E. M. Kazaryan, and L. S. Petrosyan, "Electronic states in quantum dots with ellipsoidal symmetry," *Physica E*, vol. 28, no. 4, pp. 333–338, 2005.

[4] K. G. Dvoyan, D. B. Hayrapetyan, E. M. Kazaryan, and A. A. Tshantshapanyan, "Electron states and light absorption in strongly oblate and strongly prolate ellipsoidal quantum dots in presence of electrical and magnetic fields," *Nanoscale Research Letters*, vol. 2, no. 12, pp. 601–608, 2007.

[5] Y.-H. Liu, F.-H. Yang, and S.-L. Feng, "Geometrical-confinement effects on two electrons in elliptical quantum dots," *Journal of Applied Physics*, vol. 101, no. 6, Article ID 063714, 2007.

[6] A. Benahmed, A. Aissat, and M. A. Benammar, "Optical transitions in quantum dots," *International Journal of Physics*, vol. 2, no. 4, pp. 109–111, 2014.

[7] M. Sovizi and M. Mohsseni, "Numerical calculation of eigen functions and energy levels of quantum wells, based on boundary element method," *University Politehnica of Bucharest Scientific Bulletin-Series A-Applied Mathematics and Physics*, vol. 76, no. 2, pp. 169–180, 2014.

[8] D. Zhou and A. Lorke, "Wave functions of elliptical quantum dots in a magnetic field," *American Journal of Physics*, vol. 83, no. 3, pp. 205–209, 2014.

[9] C.-H. Teng, L. Zhang, T. A. Hill, B. Demory, H. Deng, and P.-C. Ku, "Elliptical quantum dots as on-demand single photons sources with deterministic polarization states," *Applied Physics Letters*, vol. 107, no. 19, Article ID 191105, 2015.

[10] A. Halder and V. V. Kresin, "Energies and densities of electrons confined in elliptical and ellipsoidal quantum dots," *Journal of Physics: Condensed Matter*, vol. 28, no. 39, Article ID 395302, 2016.

[11] M. A. Londoño, J. H. Rúa, J. D. Giraldo-Gómez, H. Montegranario, M. E. Mora-Ramos, and C. A. Duque, "A meshless scheme for the calculation of electron and hole states in laterally coupled GaAs-$Ga_{1-x}Al_xAs$ quantum dots under applied electric field," *Superlattices and Microstructures*, vol. 87, pp. 77–82, 2016.

[12] W.-W. Gao and Z.-G. Wang, "A meshless scheme for partial differential equations based on multiquadric trigonometric B-spline quasi-interpolation," *Chinese Physics B*, vol. 23, no. 11, Article ID 110207, 2014.

[13] A. A. Gusev, O. Chuluunbaatar, S. I. Vinitsky, E. M. Kazaryan, and H. A. Sarkisyan, "The application of adiabatic method for the description of impurity states in quantum nanostructures," *Journal of Physics: Conference Series*, vol. 248, Article ID 012047, 2010.

[14] A. A. Gusev, L. L. Hai, S. I. Vinitsky et al., "Analytical and numerical calculations of spectral and optical characteristics of spheroidal quantum dots," *Physics of Atomic Nuclei*, vol. 76, no. 8, pp. 1033–1055, 2013.

[15] S. Y. López, N. Porras-Montenegro, and C. A. Duque, "Hydrostatic pressure effects on donor-related absorption spectra in GaAs-$Ga_{1-x}Al_xAs$ quantum wells," *Physica B: Condensed Matter*, vol. 362, no. 1–4, pp. 41–49, 2005.

[16] H. M. Baghramyan, M. G. Barseghyan, A. A. Kirakosyan, R. L. Restrepo, M. E. Mora-Ramos, and C. A. Duque, "Donor impurity-related linear and nonlinear optical absorption coefficients in GaAs/$Ga_{1-x}Al_xAs$ concentric double quantum rings: effects of geometry, hydrostatic pressure, and aluminum concentration," *Journal of Luminescence*, vol. 145, pp. 676–683, 2014.

[17] H. O. Oyoko, N. Porras-Montenegro, S. Y. López, and C. A. Duque, "Comparative study of the hydrostatic pressure and temperature effects on the impurity-related optical properties in single and double GaAs-$Ga_{1-x}Al_xAs$ quantum wells," *Physica Status Solidi (C) Current Topics in Solid State Physics*, vol. 4, no. 2, pp. 298–300, 2007.

[18] M. G. Barseghyan, A. K. Manaselyan, D. Laroze, and A. A. Kirakosyan, "Impurity-modulated Aharonov-Bohm oscillations and intraband optical absorption in quantum dot-ring nanostructures," *Physica E: Low-Dimensional Systems and Nanostructures*, vol. 81, pp. 31–36, 2016.

[19] M. G. Barseghyan, A. A. Kirakosyan, and D. Laroze, "Laser driven intraband optical transitions in two-dimensional quantum dots and quantum rings," *Optics Communications*, vol. 383, article 571, 2017.

[20] G. Liao and W. Xie, "Linear and nonlinear susceptibilities of a D_- system in a semiconductor quantum ring," *Superlattices and Microstructures*, vol. 82, pp. 82–89, 2015.

[21] K. Li, K. Guo, and L. Liang, "Effect of the shape of quantum dots on the refractive index changes," *Physica B: Condensed Matter*, vol. 502, pp. 146–150, 2016.

[22] F. Hecht, "New development in freefem++," *Journal of Numerical Mathematics*, vol. 20, no. 3-4, pp. 251–265, 2012.

[23] D. Ahn and S.-L. Chuang, "Calculation of linear and nonlinear intersubband optical absorptions in a quantum well model with an applied electric field," *IEEE Journal of Quantum Electronics*, vol. 23, no. 12, pp. 2196–2204, 1987.

[24] N. Zeiri, N. Sfina, S. Abdi-Ben Nasrallah, and M. Said, "Intersubband resonant enhancement of the nonlinear optical properties in asymmetric (CdS/ZnSe)/X-BeTe based quantum wells," *Optical Materials*, vol. 35, no. 5, pp. 875–880, 2013.

[25] A. Radu, N. Eseanu, and A. Spandonide, "Tuning a conventional quantum well laser by nonresonant laser field dressing of the active layer," *Physics Letters, Section A: General, Atomic and Solid State Physics*, vol. 378, no. 45, pp. 3308–3314, 2014.

[26] V. Tulupenko, C. A. Duque, V. Akimov et al., "On intersubband absorption of radiation in delta-doped QWs," *Physica E: Low-Dimensional Systems and Nanostructures*, vol. 74, pp. 400–406, 2015.

[27] M. Virgilio, D. Sabbagh, M. Ortolani, L. Di Gaspare, G. Capellini, and M. De Seta, "Physical mechanisms of intersubband-absorption linewidth broadening in s -Ge/SiGe quantum wells," *Physical Review B—Condensed Matter and Materials Physics*, vol. 90, no. 15, Article ID 155420, 2014.